

# On the regularization of impact without collision: the Painlevé paradox and compliance

S. J. Hogan and K. Uldall Kristiansen\*

January 26, 2022

## Abstract

We consider the problem of a rigid body, subject to a unilateral constraint, in the presence of Coulomb friction. We regularize the problem by assuming compliance (with both stiffness and damping) at the point of contact, for a general class of normal reaction forces. Using a rigorous mathematical approach, we recover impact without collision (IWC) in both the inconsistent and indeterminate Painlevé paradoxes, in the latter case giving an exact formula for conditions that separate IWC and lift-off. We solve the problem for arbitrary values of the compliance damping and give explicit asymptotic expressions in the limiting cases of small and large damping, all for a large class of rigid bodies.

**Keywords**— Painlevé paradox, impact without collision, compliance, regularization

## 1 Introduction

In mechanics, in problems with unilateral constraints in the presence of friction, the rigid body assumption can result in the governing equations having multiple solutions (the *indeterminate* case) or no solutions (the *inconsistent* case). The classical example of Painlevé [29, 30, 31], consisting of a slender rod slipping<sup>1</sup> along a rough surface (see Fig. 1), is the simplest and most studied example of these phenomena, now known collectively as *Painlevé paradoxes* [2, 4, 5, 32, 34]. Such paradoxes can occur at physically realistic parameter values in many important engineering systems [22, 23, 25, 27, 28, 36, 38].

When a system has no *consistent* solution, it can not remain in that state. Lecornu [21] proposed a jump in vertical velocity to escape an inconsistent, horizontal velocity, state. This jump has been called *impact without collision* (IWC) [12], *tangential impact* [13] or *dynamic jamming* [28]. Experimental evidence of IWC is given in [38].

---

\*S. J. Hogan: Department of Engineering Mathematics, University of Bristol, Bristol BS8 1UB, United Kingdom. K. Uldall Kristiansen: Department of Applied Mathematics and Computer Science, Technical University of Denmark, 2800 Kgs. Lyngby, DK.

<sup>1</sup>We prefer to avoid describing this phase of the motion as *sliding* because we will be using ideas from piecewise smooth systems [11], where sliding has exactly the opposite meaning.

IWC occurs instantaneously. So it must be incorporated into the rigid body formulation [6, 15] by considering the equations of motion in terms of the normal impulse, rather than time. However, this process has been controversial [3, 35], because it can sometimes lead to an apparent energy gain in the presence of friction.

Génot and Brogliato [12] considered the dynamics around a critical point, corresponding to zero vertical acceleration of the end of the rod. They proved that, when starting in a consistent state, the rod must stop slipping before reaching the critical point. In particular, paradoxical situations cannot be reached after a period of slipping.

One way to address the Painlevé paradox is to *regularize* the rigid body formalism. Physically this often corresponds to assuming some sort of compliance at the contact point  $A$ , typically thought of as a spring, with stiffness (and sometimes damping) that tend to the rigid body model in a suitable limit. Mathematically, very little rigorous work has been done on how IWC and Painlevé paradoxes can be regularized. Dupont and Yamajako [7] treated the problem as a slow fast system, as we will do. They explored the fast time scale dynamics, which is unstable for the Painlevé paradoxes. Song *et al.* [33] established conditions under which these dynamics can be stabilized. Le Suan An [1] considered a system with bilateral constraints and showed qualitatively the presence of a regularized IWC as a jump in vertical velocity from a compliance model with diverging stiffness. Zhao *et al.* [37] considered the example in Fig. 1 and regularized the equations by assuming a compliance that consisted of an *undamped* spring. They estimated, as a function of the stiffness, the orders of magnitude of the time taken in each phase of the (regularized) IWC. Another type of regularization was considered by Neimark and Smirnova [26] who assumed that the normal and tangential reactions took (different) finite times to adjust.

In this paper, we present the first rigorous analysis of the regularized rigid body formalism, in the presence of compliance with both stiffness *and* damping. We recover impact without collision (IWC) in both the inconsistent and indeterminate cases and, in the latter case, we present a formula for conditions that separate IWC and lift-off. We solve the problem for arbitrary values of the compliance damping and give explicit asymptotic expressions in the limiting cases of small and large damping. Our results apply directly to a general class of rigid bodies. Our approach is similar to that used in [16, 17] to understand the forward problem in piecewise smooth (PWS) systems in the presence of a two-fold.

The paper is organized as follows. In Section 2, we introduce the problem, outline some of the main results known to date and include compliance. In Section 3, we give a summary of our main results, Theorem 1 and Theorem 2, before presenting their derivation in Sections 4 and 5. We discuss our results in Section 6 and outline our conclusions in Section 7.

## 2 Classical Painlevé problem

Consider a rigid rod  $AB$ , slipping on a rough horizontal surface, as depicted in Fig. 1.

The rod has mass  $m$ , length  $2l$ , the moment of inertia of the rod about its center of mass  $S$  is given by  $I$  and its center of mass coincides with its center of gravity. The point  $S$  has coordinates  $(X, Y)$  relative to an inertial frame of reference  $(x, y)$  fixed in the rough surface. The rod makes an angle  $\theta$  with respect to the horizontal, with  $\theta$  increasing in a clockwise direction. At  $A$ , the rod experiences a contact force  $(F_T, F_N)$ , which opposes the motion.

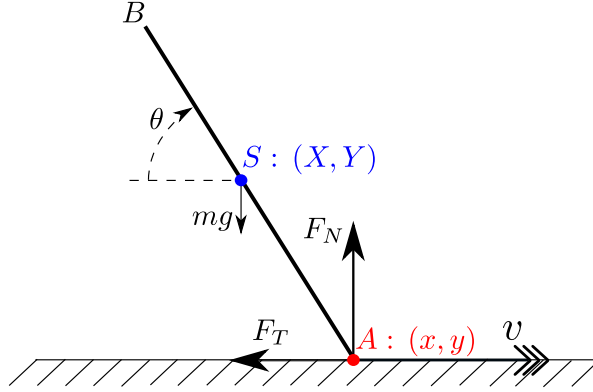


Figure 1: The classical Painlevé problem.

The dynamics of the rod is then governed by the following equations

$$\begin{aligned} m\ddot{X} &= -F_T, \\ m\ddot{Y} &= -mg - F_N, \\ I\ddot{\theta} &= -l(\cos\theta F_N - \sin\theta F_T). \end{aligned} \tag{1}$$

where  $g$  is the acceleration due to gravity.

The coordinates  $(X, Y)$  and  $(x, y)$  are related geometrically as follows

$$\begin{aligned} x &= X + l \cos \theta, \\ y &= Y - l \sin \theta. \end{aligned} \tag{2}$$

We now adopt the scalings  $(X, Y) = l(\tilde{X}, \tilde{Y})$ ,  $(x, y) = l(\tilde{x}, \tilde{y})$ ,  $(F_T, F_N) = mg(\tilde{F}_T, \tilde{F}_N)$ ,  $t = \frac{1}{\omega}\tilde{t}$ ,  $\alpha = \frac{ml^2}{I}$  where  $\omega^2 = \frac{g}{l}$ . For a uniform rod,  $I = \frac{1}{3}ml^2$ , and so  $\alpha = 3$  in this case.

Then for general  $\alpha$ , (1) and (2) can be combined to become, on dropping the tildes,

$$\begin{aligned} \ddot{x} &= -\dot{\theta}^2 \cos \theta + \alpha \sin \theta \cos \theta F_N - (1 + \alpha \sin^2 \theta) F_T, \\ \ddot{y} &= -1 + \dot{\theta}^2 \sin \theta + (1 + \alpha \cos^2 \theta) F_N - \alpha \sin \theta \cos \theta F_T, \\ \ddot{\theta} &= -\alpha(\cos \theta F_N - \sin \theta F_T). \end{aligned} \tag{3}$$

To proceed, we need to determine the relationship between  $F_N$  and  $F_T$ . We assume Coulomb friction between the rod and the surface. Hence, when  $\dot{x} \neq 0$ , we set

$$F_T = \mu \text{sign}(\dot{x}) F_N, \tag{4}$$

where  $\mu$  is the coefficient of friction. By substituting (4) into (3), we obtain two sets of

governing equations for the motion, depending on the sign of  $\dot{x}$ , as follows:

$$\begin{aligned}\dot{x} &= v, \\ \dot{v} &= a(\theta, \phi) + q_{\pm}(\theta)F_N, \\ \dot{y} &= w, \\ \dot{w} &= b(\theta, \phi) + p_{\pm}(\theta)F_N, \\ \dot{\theta} &= \phi, \\ \dot{\phi} &= c_{\pm}(\theta)F_N,\end{aligned}\tag{5}$$

where the variables  $v, w, \phi$  denote velocities in the  $x, y, \theta$  directions respectively and

$$\begin{aligned}a(\theta, \phi) &= -\phi^2 \cos \theta, \\ b(\theta, \phi) &= -1 + \phi^2 \sin \theta, \\ q_{\pm}(\theta) &= \alpha \sin \theta \cos \theta \mp \mu(1 + \alpha \sin^2 \theta), \\ p_{\pm}(\theta) &= 1 + \alpha \cos^2 \theta \mp \mu \alpha \sin \theta \cos \theta, \\ c_{\pm}(\theta) &= -\alpha(\cos \theta \mp \mu \sin \theta)\end{aligned}\tag{6}$$

for the configuration in Fig. 1. The suffices  $q_{\pm}, p_{\pm}, c_{\pm}$  correspond to  $\dot{x} = v \gtrless 0$  respectively.

System (5) is a Filippov system [11]. Hence we obtain a well-defined forward flow when  $\dot{x} = v = 0$  and

$$a(\theta, \phi) + q_+(\theta)F_N < 0 < a(\theta, \phi) + q_-(\theta)F_N,\tag{7}$$

where  $\dot{v}$  in (5) $_{\pm}$  for  $v \gtrless 0$  both oppose  $v = 0$ , by using the Filippov vector-field [11]. Simple computations give:

**Proposition 1** *The Filippov vector-field, within the subset of the switching manifold  $\dot{x} = v = 0$  where (7) holds, is given by*

$$\begin{aligned}\dot{y} &= w, \\ \dot{w} &= b(\theta, \phi) + S_w(\theta)F_N, \\ \dot{\theta} &= \phi, \\ \dot{\phi} &= S_{\phi}(\theta)F_N,\end{aligned}\tag{8}$$

where

$$\begin{aligned}S_w(\theta) &= \frac{q_-(\theta)}{q_-(\theta) - q_+(\theta)}p_+(\theta) - \frac{q_+(\theta)}{q_-(\theta) - q_+(\theta)}p_-(\theta) = \frac{1 + \alpha}{1 + \alpha \sin^2 \theta}, \\ S_{\phi}(\theta) &= \frac{q_-(\theta)}{q_-(\theta) - q_+(\theta)}c_+(\theta) - \frac{q_+(\theta)}{q_-(\theta) - q_+(\theta)}c_-(\theta) = -\frac{\alpha \cos \theta}{1 + \alpha \sin^2 \theta}.\end{aligned}\tag{9}$$

**Remark 1** Our results hold for mechanical systems with different  $q_{\pm}, p_{\pm}$  and  $c_{\pm}$  in (6) and even dependency on several angles  $\theta \in \mathbb{T}^d$ , e.g. the two-link mechanism of Zhao *et al.* [38]. Note that both  $S_w$  and  $S_{\phi}$  in (9) are independent of  $\mu$ , even for general  $c_{\pm}, q_{\pm}$  and  $p_{\pm}$ .  $\square$

In order to solve (5) and (8), we need to determine  $F_N$ . The constraint-based method leads to the Painlevé paradox. The compliance-based method is the subject of this paper.

## 2.1 Constraint-based method

In order that the constraint  $y = 0$  be maintained,  $\ddot{y}$  ( $= \dot{w}$ ) and  $F_N$  form a complementarity pair given by

$$\dot{w} \geq 0, \quad F_N \geq 0, \quad F_N \cdot \dot{w} = 0. \quad (10)$$

Note that  $F_N \geq 0$  since the rough surface can only push, not pull, the rod. Then for general motion of the rod,  $F_N$  and  $y$  satisfy the complementarity conditions

$$0 \leq F_N \perp y \geq 0. \quad (11)$$

In other words, at most one of  $F_N$  and  $y$  can be positive.

For the system shown in Fig. 1, the Painlevé paradox occurs when  $v > 0$  and  $\theta \in (0, \frac{\pi}{2})$ , provided  $p_+(\theta) < 0$ , as follows: From the fourth equation in (5), we can see that  $b$  is the free acceleration of the end of the rod. Therefore if  $b > 0$ , lift-off is always possible when  $y = 0$ ,  $w = 0$ . But if  $b < 0$ , in equilibrium we would expect a forcing term  $F_N$  to maintain the rod on  $y = 0$ . From  $\dot{w} = 0$  we obtain

$$F_N = -\frac{b}{p_+} \quad (12)$$

since  $v > 0$ . If  $p_+ > 0$ , which is always true for  $\theta \in (\frac{\pi}{2}, \pi)$ , then  $F_N \geq 0$ , in line with (11). But if  $p_+ < 0$ , which can happen if  $\theta \in (0, \frac{\pi}{2})$ , then  $F_N < 0$  in (12). Then  $F_N$  is in an *inconsistent* (or *non-existent*) mode. On the other hand, if  $b > 0$  and  $p_+ < 0$  then  $F_N > 0$  in (12). At the same time lift-off is also possible from  $y = 0$  and hence  $F_N$  is in an *indeterminate* (or *non-unique*) mode. It is straightforward to show that  $p_+(\theta) < 0$  requires

$$\mu > \mu_P(\alpha) \equiv \frac{2}{\alpha} \sqrt{1 + \alpha}. \quad (13)$$

Then the Painlevé paradox can occur for  $\theta \in (\theta_1, \theta_2)$  where

$$\begin{aligned} \theta_1(\mu, \alpha) &= \arctan \frac{1}{2} \left( \mu\alpha - \sqrt{\mu^2\alpha^2 - 4(1 + \alpha)} \right), \\ \theta_2(\mu, \alpha) &= \arctan \frac{1}{2} \left( \mu\alpha + \sqrt{\mu^2\alpha^2 - 4(1 + \alpha)} \right). \end{aligned} \quad (14)$$

For a uniform rod with  $\alpha = 3$ , we have  $\mu_P(3) = \frac{4}{3}$ . For  $\alpha = 3$  and  $\mu = 1.4$  the dynamics can be summarized<sup>2</sup> in the  $(\theta, \phi)$ -plane, as in Fig. 2. Along  $\theta = \theta_1, \theta_2$ , we have  $p_+(\theta) = 0$ . These lines intersect the curve  $b(\theta, \phi) = 0$  at four points:  $\phi_{1,2}^\pm = \pm \sqrt{\csc \theta_{1,2}}$ . Génot and Brogliato [12] showed that the point  $P : (\theta, \phi) = (\theta_1, \sqrt{\csc \theta_1})$  is the most important and analyzed the local dynamics around it. The rigid body equations (1) are unable to resolve the dynamics in the third and fourth quadrants. So we regularize these equations using compliance.

---

<sup>2</sup>Compare with Figure 2 of Génot and Brogliato [12], where the authors plot the *unscaled* angular velocity  $\omega\phi$  vs.  $\theta$ , for the case  $g = 9.8 \text{ ms}^{-2}$ ,  $l = 1 \text{ m}$ .

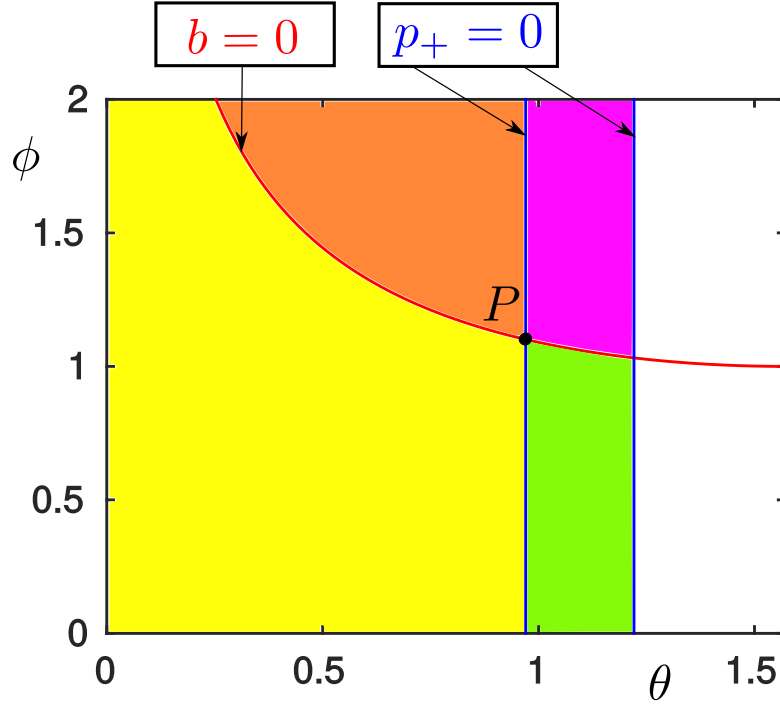


Figure 2: The  $(\theta, \phi)$ -plane for the classical Painlevé problem of Fig. 1, for  $\alpha = 3$  and  $\mu = 1.4$ . The point  $P$  has coordinates  $(\theta_1, \sqrt{\csc \theta_1})$ , where  $\theta_1$  is given in (14). In the first quadrant centered on  $P$ , we have  $b > 0$ ,  $p_+ < 0$ , so the dynamics is indeterminate (non-unique). In the second quadrant,  $b > 0$ ,  $p_+ > 0$  and the rod lifts off the rough surface. In the third quadrant,  $b < 0$ ,  $p_+ > 0$  and the rod moves (slips) along the surface. Here Génot and Brogliato [12] showed that the dynamics cannot cross  $p_+ = 0$  unless also  $b = 0$ . In the fourth quadrant,  $b < 0$ ,  $p_+ < 0$  and the dynamics is inconsistent (non-existent). Even though the constraint  $y = 0$  is satisfied, there exists no positive value of  $F_N$ , contradicting (11).

## 2.2 Compliance-based method

We assume that there is compliance at the point  $A$  between the rod and the surface, when they are in contact (see Fig. 1). Following [7, 24], we assume that there are small excursions into  $y < 0$ . Then we require that the nonnegative normal force  $F_N(y, w)$  is a PWS function of  $(y, w)$ :

$$F_N(y, w) = [f(y, w)] \equiv \begin{cases} 0 & \text{for } y > 0 \\ \max\{f(y, w), 0\} & \text{for } y \leq 0, \end{cases} \quad (15)$$

where the operation  $[\cdot]$  is defined by the last equality and  $f(y, w)$  is assumed to be a smooth function of  $(y, w)$  satisfying  $\partial_y f < 0, \partial_w f < 0$ . The quantities  $\partial_y f(0, 0)$  and  $\partial_w f(0, 0)$  represent a (scaled) spring constant and damping coefficient, respectively. We are interested in the case when the compliance is very large, so we introduce a small parameter  $\epsilon$  as follows:

$$\partial_y f(0, 0) = \epsilon^{-2}, \quad \partial_w f(0, 0) = \epsilon^{-1} \delta. \quad (16)$$

This choice of scaling [7, 24] ensures that the critical damping coefficient ( $\delta_{crit} = 2$  in the classical Painlevé problem) is independent of  $\epsilon$ . Our analysis can handle any  $f$  of the form  $f(y, w) = \epsilon^{-1}h(\epsilon^{-1}y, w)$  with

$$h(\hat{y}, w) = -\hat{y} - \delta w + \mathcal{O}((\hat{y} + w)^2). \quad (17)$$

But, to obtain our quantitative results, we truncate (17) and consider the linear function

$$h(\hat{y}, w) = -\hat{y} - \delta w, \quad (18)$$

so that

$$F_N(y, w) = \epsilon^{-1} [-\epsilon^{-1}y - \delta w]. \quad (19)$$

In what follows, the first equation in (5) will play no role, so we drop it from now on. Then we combine the remaining five equations in (5) with (15) and (16) to give the following set of governing equations that we will use in the sequel

$$\begin{aligned} \dot{y} &= w, \\ \dot{w} &= b(\theta, \phi) + p_{\pm}(\theta)\epsilon^{-1}[-\epsilon^{-1}y - \delta w], \\ \dot{\theta} &= \phi, \\ \dot{\phi} &= c_{\pm}(\theta)\epsilon^{-1}[-\epsilon^{-1}y - \delta w], \\ \dot{v} &= a(\theta, \phi) + q_{\pm}(\theta)\epsilon^{-1}[-\epsilon^{-1}y - \delta w], \end{aligned} \quad (20)$$

For  $\epsilon > 0$  this is a well-defined Filippov system. The slipping region (7) and the Filippov vector-field (8) are obtained by replacing  $F_N$  in these expressions with the square bracket  $\epsilon^{-1}[-\epsilon^{-1}y - \delta w]$  (see also Lemma 5 below).

### 3 Main Results

We now present the main results of our paper, Theorem 1 and Theorem 2. Theorem 1 shows that, if the rod starts in the fourth quadrant of Fig. 2, it undergoes a (regularized) IWC for a time of  $\mathcal{O}(\epsilon \ln \epsilon^{-1})$ . The same theorem also gives expressions for the resulting vertical velocity of the rod in terms of the compliance damping and initial horizontal velocity and orientation of the rod.

**Theorem 1** *Consider an initial condition*

$$(y, w, \theta, \phi, v) = (0, \mathcal{O}(\epsilon), \theta_0, \phi_0, v_0), \quad v_0 > 0, \quad (21)$$

*within the region of inconsistency (non-existence) where*

$$p_+(\theta_0) < 0, \quad b(\theta_0, \phi_0) < 0, \quad (22)$$

and  $q_+(\theta_0) < 0$ ,  $q_-(\theta_0) > 0$ ,  $a \neq 0$ . Then the forward flow of (21) under (20) returns to  $\{(y, w, \theta, \phi, v) | y = 0\}$  after a time  $\mathcal{O}(\epsilon \ln \epsilon^{-1})$  with

$$\begin{aligned} w &= e(\delta, \theta_0)v_0 + o(1), \\ \theta &= \theta_0 + o(1), \\ \phi &= \phi_0 + \left\{ -\frac{c_+(\theta_0)}{q_+(\theta_0)} + \frac{S_\phi(\theta_0)}{S_w(\theta_0)} \left( e(\delta, \theta_0) + \frac{p_+(\theta_0)}{q_+(\theta_0)} \right) \right\} v_0 + o(1), \\ v &= o(1), \end{aligned} \tag{23}$$

as  $\epsilon \rightarrow 0$ . During this time  $y = \mathcal{O}(\epsilon)$ ,  $w = \mathcal{O}(1)$  so that  $F_N = \mathcal{O}(\epsilon^{-1})$ . The function  $e(\delta, \theta_0)$ , given in (61) below, is smooth and monotonic in  $\delta$  and has the following asymptotic expansions:

$$e(\delta, \theta_0) = \frac{p_-(\theta_0) - p_+(\theta_0)}{q_-(\theta_0)p_+(\theta_0) - q_+(\theta_0)p_-(\theta_0)} \delta^{-2} (1 + \mathcal{O}(\delta^{-2} \ln \delta^{-1})) \quad \text{for } \delta \gg 1, \tag{24}$$

$$\begin{aligned} e(\delta, \theta_0) &= \sqrt{\frac{p_+(\theta_0)(p_-(\theta_0) - p_+(\theta_0))}{q_+(\theta_0)(q_-(\theta_0) - q_+(\theta_0))}} \left( 1 - \right. \\ &\quad \left. \frac{\sqrt{S_w(\theta_0)}}{2} \left( \pi - \arctan \left( \sqrt{-\frac{S_w(\theta_0)}{p_+(\theta_0)}} \right) \right) \delta + \mathcal{O}(\delta^2) \right) \quad \text{for } \delta \ll 1. \end{aligned} \tag{25}$$

□

Theorem 2 is similar to Theorem 1, but now the rod starts in the first quadrant of Fig. 2. This theorem also gives an exact formula for initial conditions that separate (regularized) IWC and lift off.

**Theorem 2** Consider an initial condition

$$(y, w, \theta, \phi, v) = (0, \epsilon w_{10}, \theta_0, \phi_0, v_0), \quad w_{10} < w_{1*} \equiv -\lambda_-(\theta_0) \frac{b(\theta_0, \phi_0)}{p_+(\theta_0)} < 0, \tag{26}$$

with  $\lambda_-$  defined in (33) below, within the region of indeterminacy (non-uniqueness) where

$$p_+(\theta_0) < 0, \quad b(\theta_0, \phi_0) > 0, \tag{27}$$

and  $q_+(\theta_0) < 0$ ,  $q_-(\theta_0) > 0$ ,  $a \neq 0$ . Then the conclusions of Theorem 1, including expressions (23), (24) and (25), still hold true as  $\epsilon \rightarrow 0$ . For  $w_{10} > w_{1*}$  lift-off occurs directly after a time  $\mathcal{O}(\epsilon)$  with  $w = \mathcal{O}(\epsilon)$ . During this period  $y = \mathcal{O}(\epsilon^2)$ , so  $F_N = \mathcal{O}(1)$ . □

**Remark 2** These two theorems have not appeared before in the literature. In the rigid body limit ( $\epsilon \rightarrow 0$ ), we recover IWC in both cases. Previous authors have either not carried out the “very difficult” calculation [24], performed numerical calculations [5, 7] or given a range of estimates for the time of (regularized) IWC in the *absence* of damping [37]. We give exact and asymptotic expressions for key quantities as well as providing a geometric interpretation of our results, for a large class of rigid bodies, in the presence of a large class of normal forces, as well as giving a precise estimate for the time of (regularized) IWC, all in the presence of both stiffness and damping. Note that we are not attempting to describe all the dynamics around  $P$ . There is a canard connecting the third quadrant with the first and the analysis is exceedingly complicated [18] due to fast oscillatory terms. Instead, we follow [37] and consider that the rod dynamics starts in a configuration with  $p_+(\theta_0) < 0$ . □



## 4 Proof of Theorem 1: IWC in the inconsistent case

The proof of Theorem 1 is divided into three phases, illustrated in Fig. 3. These phases are a generalisation of the phases of IWC in its rigid body formulation [38].

- Slipping compression (section 4.2): During this phase  $y$ ,  $w$  and  $v$  all decrease. The dynamics follow an unstable manifold  $\gamma^u$  of a set of critical points  $C$ , given in (31) below, as  $\epsilon \rightarrow 0$ . Along  $\gamma^u$  the normal force  $F_N = \mathcal{O}(\epsilon^{-1})$  and  $v$  will therefore quickly decrease to 0. Mathematically this part is complicated by the fact that the initial condition (21) belongs to the critical set  $C$  as  $\epsilon \rightarrow 0$ .
- Sticking (section 4.3): Since  $F_N = \mathcal{O}(\epsilon^{-1})$  and  $q_+q_- < 0$  the rod will stick with  $v \equiv 0$ . During this phase  $\ddot{y} = \dot{w} > 0$  and eventually sticking ends with  $F_N = 0$  as  $\epsilon \rightarrow 0$ .
- Lift-off (section 4.4): In the final phase  $F_N = 0$ , lift off occurs and the system eventually returns to  $y = 0$ .

### 4.1 Slow-fast setting: Initial scaling

Before we consider the first phase of IWC, we apply the scaling

$$y = \epsilon \hat{y}, \quad (28)$$

also used in [7, 24], which brings the two terms in (19) to the same order. Now let

$$\hat{F}_N(\hat{y}, w) \equiv \epsilon F_N(\epsilon \hat{y}, w) = [-\hat{y} - \delta w]. \quad (29)$$

Equations (20) then read:

$$\begin{aligned} \hat{y}' &= w, \\ w' &= \epsilon b(\theta, \phi) + p_{\pm}(\theta) \hat{F}_N(\hat{y}, w), \\ \theta' &= \epsilon \phi, \\ \phi' &= c_{\pm}(\theta) \hat{F}_N(\hat{y}, w), \\ v' &= \epsilon a(\theta, \phi) + q_{\pm}(\theta) \hat{F}_N(\hat{y}, w), \end{aligned} \quad (30)$$

with respect to the *fast time*  $\tau = \epsilon^{-1}t$  where  $()' = \frac{d}{d\tau}$ . This is a slow-fast system in non-standard form [24]. Only  $\theta$  is truly slow whereas  $(\hat{y}, w, \phi, v)$  are all fast. But the set of critical points

$$C = \{(\hat{y}, w, \theta, \phi, v) | \hat{y} = 0, w = 0\}, \quad (31)$$

for  $\epsilon = 0$  is just three dimensional. System (30) is PWS [16, 17]. We now show that  $(30)_+$  contains stable and unstable manifolds  $\gamma^{s,u}$  when the equivalent rigid body equations exhibit a Painlevé paradox, when  $p_+(\theta_0) < 0$ . The saddle structure of  $C$  within the fourth quadrant has been recognized before [1, 7, 33].

**Proposition 2** Consider the system  $(30)_+$ . Then for  $p_+(\theta_0) < 0$  there exist smooth stable and unstable sets  $\gamma^{s,u}(\theta_0, \phi_0, v_0)$ , respectively, of  $(\hat{y}, w, \theta, \phi, v) = (0, 0, \theta_0, \phi_0, v_0) \in C$  contained within  $\hat{F}_N \geq 0$  given by

$$\gamma^{s,u}(\theta_0, \phi_0, v_0) = \left\{ (\hat{y}, w, \theta, \phi, v) \mid \begin{aligned} w &= \lambda_{\mp} \hat{y}, \quad \theta = \theta_0, \quad \phi = \phi_0 - c_+(\theta_0) \lambda_{\mp}^{-1} [1 + \delta \lambda_{\mp}] \hat{y}, \\ v &= v_0 + \frac{q_+(\theta_0)}{p_+(\theta_0)} \lambda_{\mp}(\theta_0) \hat{y}, \quad \hat{y} \leq 0 \end{aligned} \right\}, \quad (32)$$

with  $\lambda_{\mp}(\theta_0) \leq 0$  given in (33) below.  $\square$

**PROOF** Consider the smooth system,  $(30)_{\hat{F}_N = -\hat{y} - \delta w}$ , obtained from (30) by setting  $\hat{F}_N = -\hat{y} - \delta w$ . The linearization of  $(30)_{\hat{F}_N = -\hat{y} - \delta w}$  about a point in  $C$  then only has two non-zero eigenvalues:

$$\lambda_{\pm}(\theta) = -\frac{\delta p_+(\theta)}{2} \pm \frac{1}{2} \sqrt{\delta^2 p_+(\theta)^2 - 4p_+(\theta)}, \quad (33)$$

satisfying

$$\lambda_{\pm}^2 = -p_+(\theta) (1 + \delta \lambda_{\pm}). \quad (34)$$

For  $p_+(\theta) < 0$  we have  $\lambda_- < 0 < \lambda_+$ . The eigenvectors associated with  $\lambda_{\pm}$  are  $v_{\pm} = \left( 1, \lambda_{\pm}, 0, \frac{c_+}{p_+(\theta)} \lambda_{\pm}, \frac{q_+}{p_+(\theta)} \lambda_{\pm} \right)^T$ . Therefore the smooth system  $(30)_{\hat{F}_N = -\hat{y} - \delta w}$  has a (stable, unstable) manifold  $\gamma^{s,u}$  tangent to  $v_{\mp}$  at  $(\hat{y}, w, \theta, \phi, v) = (0, 0, \theta_0, \phi_0, v_0)$ . But then for  $\hat{y} \leq 0$ , we have  $\hat{F}_N(\hat{y}, \lambda_{\pm} \hat{y}) = -(1 + \delta \lambda_{\pm}) \hat{y} = \frac{\lambda_{\pm}^2}{p_+(\theta)} \hat{y} \geq 0$ , by (34). Hence the restrictions of  $\gamma^{s,u}$  in (32) to  $\hat{y} < 0$  are (stable, unstable) sets of  $C$  for the PWS system  $(30)_{\hat{F}_N = [-\hat{y} - \delta w]}$ .  $\blacksquare$

**Remark 3** For the smooth system  $(30)_{\hat{F}_N = -\hat{y} - \delta w}$ , the critical manifold  $C$  perturbs by Fenichel's theory [8, 9, 10] to a smooth slow manifold  $C_{\epsilon}$ , being  $C^{\infty}$   $\mathcal{O}(\epsilon)$ -close to  $C$ . A simple calculation shows that  $C_{\epsilon} : \hat{y} = \epsilon \frac{b(\theta, \phi)}{p_+(\theta)} (1 + \mathcal{O}(\epsilon))$ ,  $w = \mathcal{O}(\epsilon^2)$ . Since  $b(\theta, \phi) < 0$  in this case,  $C_{\epsilon} \subset \{\hat{y} > 0\}$  for  $\epsilon$  sufficiently small. Therefore the manifold  $C_{\epsilon}$  is invariant for the smooth system  $(30)_{\hat{F}_N = -\hat{y} - \delta w}$  only. It is an artifact for the PWS system  $(30)_{\hat{F}_N = [-\hat{y} - \delta w]}$  since the square bracket vanishes for  $\hat{y} > 0$ , by (15).  $\square$

**Remark 4** Our arguments are geometrical and rely on hyperbolic methods of dynamical systems theory only. Therefore the results remain unchanged qualitatively if we replace the piecewise linear  $\hat{F}_N$  in (29) with the nonlinear version  $\hat{F}_N(\hat{y}, w) = [h(\hat{y}, w)]$ , where  $h(\hat{y}, w) = -\hat{y} - \delta w + \mathcal{O}((\hat{y} + w)^2)$  as in (17), having (18) as its linearization about  $\hat{y} = w = 0$ . We would obtain again a saddle-type critical set  $C$  with nonlinear (stable, unstable) manifolds  $\gamma^{s,u}$ .  $\square$

Following the initial scaling (28) of this section, we now consider the three phases of IWC.

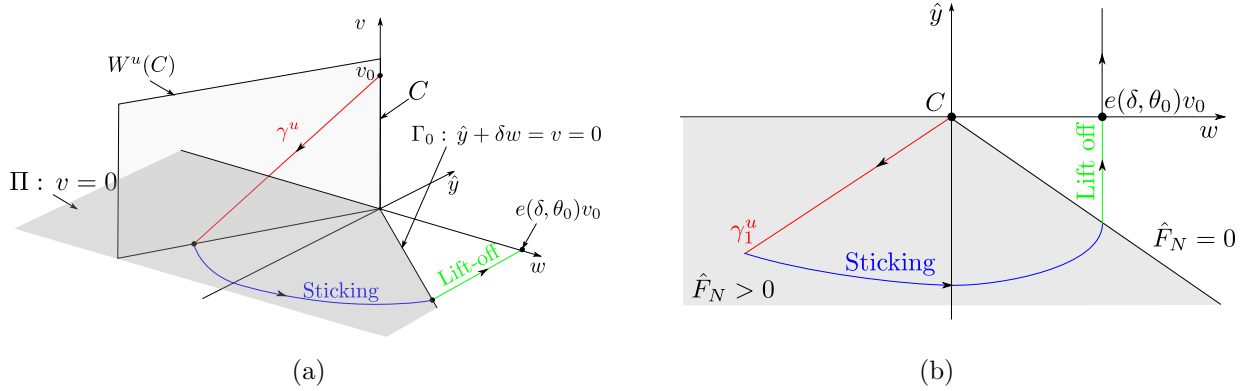


Figure 3: The limit  $\epsilon \rightarrow 0$  shown using (a) the  $(w, \hat{y}, v)$ -variables and (b) a projection onto the  $(w, \hat{y})$ -plane. The *slipping compression* phase, shown in red, where  $\hat{y}$ ,  $w$  and  $v > 0$  all decrease, is described geometrically by an unstable manifold  $\gamma^u$  (32) of a critical set  $C$ , given in (31). The *sticking* phase (in blue) is described by Filippov [11]. Finally the *lift-off* phase (in green) occurs and we return to  $\hat{y} = 0$ . In both figures the grey region is where  $\hat{F}_N > 0$ .

## 4.2 Slipping compression

Now we describe the first phase of the regularized IWC: *slipping compression*, which ends when  $v = 0$ . We define the following section (or *switching manifold*),  $\Pi$  shown in Fig. 3(a):

$$\Pi = \{(\hat{y}, w, \theta, \phi, v) | v = 0\}. \quad (35)$$

Proposition 3 describes the intersection of the forward flow of initial conditions (21) with  $\Pi$ ; in other words, the values of  $\hat{y}, w, \theta, \phi$  at the *end* of the slipping compression phase.

**Proposition 3** *The forward flow of the initial conditions (21) under (30) intersects  $\Pi$  in*

$$\gamma^u \cap \Pi + o(1) \equiv \left\{ (\hat{y}, w, \theta, \phi, 0) \mid \begin{aligned} \hat{y} &= -\frac{p_+(\theta_0)}{q_+(\theta_0)\lambda_+(\theta_0)}v_0 + o(1), & w &= -\frac{p_+(\theta_0)}{q_+(\theta_0)}v_0 + o(1) \\ \theta &= \theta_0 + o(1), & \phi &= \phi_0 - \frac{c_+(\theta_0)}{q_+(\theta_0)}v_0 + o(1), \end{aligned} \right\}, \quad (36)$$

as  $\epsilon \rightarrow 0$ . □

**Remark 5** The  $o(1)$ -term in (36) is  $\mathcal{O}(\epsilon^c)$  for any  $c \in (0, 1)$  (see also Lemma 3 below). □

### 4.2.1 Proof of Proposition 3

We prove Proposition 3 using Fenichel's normal form theory [14]. But since (30) $_{\hat{F}_N = [-\hat{y} - \delta w]}$  is piecewise smooth, care must be taken. There are at least two ways to proceed. One way is to consider the smooth system (30) $_{\hat{F}_N = -\hat{y} - \delta w}$ , then rectify  $C_\epsilon$  by straightening out its stable and unstable manifolds. Then (30) $_{\hat{F}_N = -\hat{y} - \delta w}$  will be a standard slow-fast system to which

Fenichel's normal form theory applies. Subsequently one would then have to ensure that conclusions based on the smooth  $(30)_{\hat{F}_N = -\hat{y} - \delta w}$  also extend to the PWS system  $(30)_{\hat{F}_N = [-\hat{y} - \delta w]}$ . One way to do this is to consider the following scaling

$$\kappa_1 : \quad \hat{y} = r_1 \hat{y}_1, \quad w = r_1 w_1, \quad \epsilon = r_1, \quad (37)$$

zooming in on  $C$  at  $\hat{y} = 0, w = 0$ . In terms of the original variables,  $y = \epsilon^2 \hat{y}_1, w = \epsilon w_1$ . The scalings  $(\hat{y}, w)$  and  $(\hat{y}_1, w_1)$  have both appeared in the literature [5, 7, 24].

In this paper we follow another approach (basically reversing the process described above) which works more directly with the PWS system. Therefore in Section 4.2.2 we study the scaling (37) first. We will show that the  $(\hat{y}_1, w_1)$ -system contains important geometry of the PWS system (significant, for example, for the separation of initial conditions in Theorem 2). Then in Section 4.2.3 we connect the “small”  $(\hat{y} = \mathcal{O}(\epsilon), w = \mathcal{O}(\epsilon))$  described by (37) with the “large”  $(\hat{y} = \mathcal{O}(1), w = \mathcal{O}(1))$  in (30) by considering coordinates described by the following transformation:

$$\kappa_2 : \quad \hat{y} = -r_2, \quad w = r_2 w_2, \quad \epsilon = r_2 \epsilon_2. \quad (38)$$

For  $y_1 < 0$  we have the following coordinate change  $\kappa_{21}$  between  $\kappa_1$  and  $\kappa_2$ :

$$\kappa_{21} : \quad r_2 = -r_1 y_1, \quad w_2 = -w_1 y_1^{-1}, \quad \epsilon_2 = -y_1^{-1}. \quad (39)$$

The coordinates in  $\kappa_2$  (38) appear as a *directional chart* obtained by setting  $\bar{y} = -1$  in the blowup transformation  $(r, \bar{y}, \bar{w}, \bar{\epsilon}) \mapsto (\hat{y}, w, \epsilon)$  given by<sup>3</sup>

$$\hat{y} = r \bar{y}, \quad w = r \bar{w}, \quad \epsilon = r \bar{\epsilon}, \quad r \geq 0, \quad (\bar{y}, \bar{w}, \bar{\epsilon}) \in S^2 = \{(\bar{y}, \bar{w}, \bar{\epsilon}) | \bar{y}^2 + \bar{w}^2 + \bar{\epsilon}^2 = 1\}. \quad (40)$$

The blowup is chosen so that the zoom in (37) coincides with the *scaling chart* obtained by setting  $\bar{\epsilon} = 1$ . The blowup transformation *blows up*  $C$  to  $\bar{C} : r = 0, (\bar{y}, \bar{w}, \bar{\epsilon}) \in S^2$  a space  $(\theta, \phi, v) \in \mathbb{R}^3$  of spheres.<sup>4</sup>

The main advantage of our approach is that in chart  $\kappa_2$  we can focus on  $\bar{C} \cap \{\bar{y}^{-1} \bar{w} > -\delta^{-1}, \bar{y} < 0\}$  (or simply  $w_2 < \delta^{-1}$  in (38)) of  $\bar{C}$ , the grey area in Fig. 3, where

$$r^{-1} \hat{F}_N(\hat{y}, w) = [-\bar{y} - \delta \bar{w}] = -\bar{y} \left(1 + \delta \bar{y}^{-1} \bar{w}\right) > 0, \quad (41)$$

and the system will be smooth. This enables us to apply Fenichel's normal form theory [14] there. All the necessary patching for the PWS system is done independently in the scaling chart  $\kappa_1$ . Also chart  $\kappa_2$  enables a matching between the two scalings that have appeared in the literature:  $\kappa_1 \cap \{\hat{y}_1 < 0, r_1 = 0\}$ , visible within  $r_2 = 0$  of (38), and system  $(30)_{\epsilon=0}$ , visible within  $\epsilon_2 = 0$  of (38).

<sup>3</sup>More accurately, the chart  $\bar{y} = -1$  corresponds to

$$r = r_1 \sqrt{1 + \epsilon_1^2 + w_1^2}, \quad \bar{y} = -1/\sqrt{1 + \epsilon_1^2 + w_1^2}, \quad \bar{w} = w_1/\sqrt{1 + \epsilon_1^2 + w_1^2}, \quad \bar{\epsilon} = \epsilon_1/\sqrt{1 + \epsilon_1^2 + w_1^2},$$

with  $\bar{y}^2 + \bar{w}^2 + \bar{\epsilon}^2 = 1$ . See [20] for further details on directional and scaling charts.

<sup>4</sup>Note that (40) is not a *blowup* transformation in the sense of Krupa and Szmolyan [19], where geometric blowup is applied in conjunction with desingularization to study loss of hyperbolicity in slow-fast systems. We will not desingularize the vector-field here.

#### 4.2.2 Chart $\kappa_1$

Let  $\hat{F}_{N,1}(\hat{y}_1, w_1) = \epsilon^{-1} \hat{F}_N(\epsilon \hat{y}_1, \epsilon w_1) = [-\hat{y}_1 - \delta w_1]$ . Then applying chart  $\kappa_1$  in (37) to the non-standard slow-fast system (30) gives the following equations:

$$\begin{aligned} \hat{y}_1' &= w_1, \\ w_1' &= b(\theta, \phi) + p_+(\theta) \hat{F}_{N,1}(\hat{y}_1, w_1), \\ \theta' &= \epsilon \phi, \\ \phi' &= \epsilon c_+(\theta) \hat{F}_{N,1}(\hat{y}_1, w_1), \\ v' &= \epsilon \left( a(\theta, \phi) + q_+(\theta) \hat{F}_{N,1}(\hat{y}_1, w_1) \right), \end{aligned} \quad (42)$$

Equation (42) is a slow-fast system in standard form:  $(\hat{y}_1, w_1)$  are fast variables whereas  $(\theta, \phi, v)$  are slow variables. By assumption (22) of Theorem 1,  $b < 0$ ,  $p_+ < 0$  and so, since  $\hat{F}_{N,1}(\hat{y}_1, w_1) \geq 0$ , we have  $w_1' < 0$  in (42). Hence there exists no critical set for the PWS system  $(42)_{\epsilon=0}$ . The critical set  $C_1$  of the *smooth* system  $(42)_{\hat{F}_{N,1}=-\hat{y}_1-\delta w_1}$ , given by

$$C_1 = \{(\hat{y}_1, w_1, \theta, \phi, v) | \hat{y}_1 = \frac{b(\theta, \phi)}{p_+(\theta)}, w_1 = 0\}, \quad (43)$$

lies within  $\hat{y}_1 > 0$ . So  $C_1$  is an invariant of  $(42)_{\hat{F}_{N,1}=-\hat{y}_1-\delta w_1}$  but an artifact of the PWS system  $(42)_{\hat{F}_{N,1}=-\hat{y}_1-\delta w_1}$ , as shown in Fig. 4(a) (recall also Remark 3).

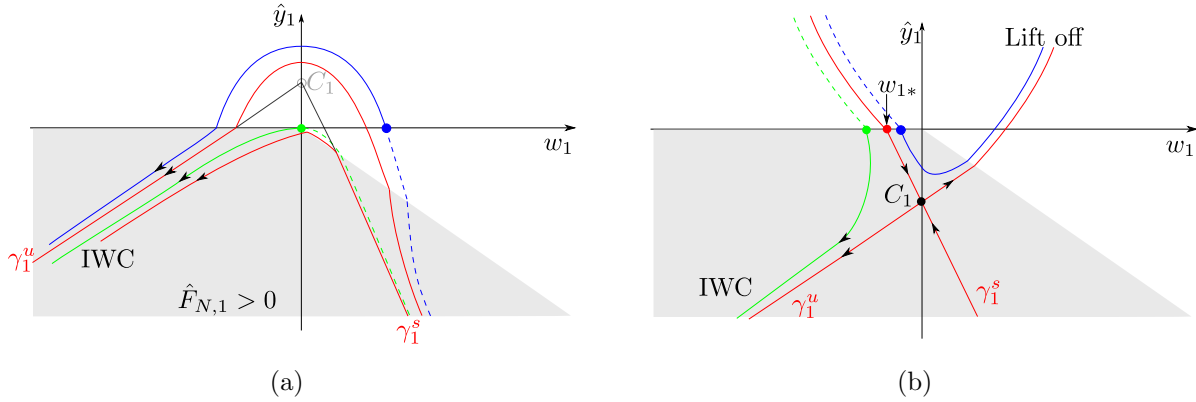


Figure 4: (a) Phase portrait  $(42)_{\epsilon=0}$  for  $b < 0$  (Theorem 1 in this Section). The critical set  $C_1$  of  $(42)_{\hat{F}_{N,1}=-\hat{y}_1-\delta w_1}$ , given by (43), is an artifact of the PWS system  $(42)_{\hat{F}_{N,1}=-\hat{y}_1-\delta w_1}$ . (b) Phase portrait  $(42)_{\epsilon=0}$  for  $b > 0$  (Theorem 2 in Section 5). Here  $C_1$  is a saddle-type critical manifold for the PWS system,  $\gamma_1^u$  is given by (44),  $\gamma_1^s$  by (64) and  $w_{1*}$  by (65). The grey region is now where  $\hat{F}_{N,1} > 0$ . Orbit segments outside this region are parabolas turning downwards and upwards in (a) and (b), respectively. Dashed lines indicate backward orbits, from initial conditions on the  $w_1$ -axis. Similar figures from numerical computations appear in [5].

The unstable manifold  $\gamma_1^u$  of  $C_1$  in the smooth system  $(42)_{\hat{F}_{N,1}=-\hat{y}_1-\delta w_1}$  is given by

$$\gamma_1^u(\theta_0, \phi_0, v_0) = \left\{ (\hat{y}_1, w_1, \theta_0, \phi_0, v_0) \mid \hat{y}_1 = \frac{b(\theta_0, \phi_0)}{p_+(\theta_0)} + s, \quad w_1 = \lambda_+(\theta_0)s, \quad s \leq -\frac{b(\theta_0, \phi_0)}{p_+(\theta_0)} \right\} \quad (44)$$

and its restriction to the subset  $\hat{y}_1 \leq 0, w_1 \leq 0$  where  $\hat{F}_{N,1} \geq 0$ , is locally invariant for the PWS system  $(42)_{\hat{F}_{N,1}=[-\hat{y}_1-\delta w_1]}$ .

In chart  $\kappa_1$ , initial conditions (21) now become:

$$(\hat{y}_1, w_1, \theta, \phi, v) = (0, \mathcal{O}(1), \theta_0, \phi_0, v_0). \quad (45)$$

In Lemma 1, we determine the values of the variables during the slipping compression phase, starting from initial conditions (45), as seen in chart  $\kappa_1$ , and show that the system remains close to  $\gamma_1^u(\theta_0, \phi_0, v_0)$ .

**Lemma 1** *Consider  $\Lambda_1 = \{(\hat{y}_1, w_1, \theta, \phi, v) \mid \hat{y}_1 = -\nu^{-1}\}$  with  $\nu > 0$  small. Then the forward flow of (45) under (42) intersects  $\Lambda_1$  in*

$$z_1(\epsilon) \equiv (-\nu^{-1}, w_{1c}(\nu) + \mathcal{O}(\epsilon), \theta_0 + \mathcal{O}(\epsilon), \phi_0 + \mathcal{O}(\epsilon), v_0 + \mathcal{O}(\epsilon)). \quad (46)$$

where  $w_{1c}(\nu) = -\lambda_+\nu^{-1}(1 + o(1))$ ,  $\nu \rightarrow 0$ . □

**PROOF** Consider the layer problem  $(42)_{\epsilon=0}$ . Then  $\theta(\tau) = \theta_0, \phi(\tau) = \phi_0, v(\tau) = v_0$ . Since  $b < 0$ , initial conditions (45) with  $w_1 > 0$  return to  $\hat{y}_1 = 0$  with  $w_1 < 0$ , see Fig. 4(a). Therefore we consider  $w_1(0) \leq 0$  subsequently. Now we solve  $(42)_{\hat{F}_{N,1}=-\hat{y}_1-\delta w_1, \epsilon=0}$  to find

$$\begin{aligned} \hat{y}_1(\tau) &= \frac{b(\theta_0, \phi_0)}{p_+(\theta_0)} + k_+e^{\lambda_+\tau} + k_-e^{\lambda_-\tau}, \\ w_1(\tau) &= k_+\lambda_+e^{\lambda_+\tau} + k_-\lambda_-e^{\lambda_-\tau}. \end{aligned} \quad (47)$$

Here  $k_+ = \frac{\lambda_-b/p_+-w_1(0)}{\lambda_+-\lambda_-} < 0, k_- = \frac{w_1(0)-\lambda_+b/p_+}{\lambda_+-\lambda_-} < 0$  depend on initial conditions. Since  $\lambda_- < 0 < \lambda_+$  the solution remains within  $\hat{F}_{N,1} > 0$  for  $\tau > 0$  and contracts towards  $\gamma_1^u(\theta_0, \phi_0, v_0)$  as  $\tau \rightarrow \infty$ . Therefore there exists a time  $\tau_c = \tau_c(\nu) > 0$  such that  $\Lambda_1$  is reached. Then at  $\tau = \tau_c$ , we have  $z_1(0) = (-\nu^{-1}, w_{1c}, \theta_0, \phi_0, v_0)$ , where  $w_{1c}(\nu) \equiv w_1(\tau_c) = k_+\lambda_+e^{\lambda_+\tau_c} + k_-\lambda_-e^{\lambda_-\tau_c} = -\lambda_+\nu^{-1}(1 + o(1)) < 0$ . To obtain  $z_1(\epsilon)$  we apply regular perturbation theory and the implicit function theorem using transversality to  $\Lambda_1$  for  $\epsilon = 0$ . ■

For  $\epsilon > 0$  the variables  $(\phi, v)$  will vary by  $\mathcal{O}(1)$ -amount as  $\hat{y}_1, w_1 \rightarrow -\infty$ . But the variables  $(\phi, v)$  are fast in (30) and slow in (42). To describe this transition we change to chart  $\kappa_2$ .

### 4.2.3 Chart $\kappa_2$

Writing the non-standard slow-fast PWS system  $(30)_{\hat{F}_N=[-\hat{y}-\delta w]}$  in chart  $\kappa_2$ , given by (38), gives the following smooth (as anticipated by (41)) system

$$\begin{aligned}\epsilon_2' &= \epsilon_2 w_2, \\ w_2' &= \epsilon_2 b(\theta, \phi) + p_+(\theta) (1 - \delta w_2) + w_2^2, \\ \theta' &= \epsilon \phi, \\ \phi' &= c_+(\theta) r_2 (1 - \delta w_2), \\ v' &= \epsilon a(\theta, \phi) + q_+(\theta) r_2 (1 - \delta w_2), \\ r_2' &= -r_2 w_2,\end{aligned}\tag{48}$$

on the box  $U_2 = \{(\epsilon_2, w_2, \theta, \phi, v, r_2) | \epsilon_2 \in [0, \nu], w_2 \in [-\lambda_+ - \rho, -\lambda_+ + \rho], r_2 \in [0, \nu]\}$ , for  $\rho > 0$  sufficiently small (so that  $w_2 < \delta^{-1}$ ) and  $\nu$  as above. Notice that  $z_1(\epsilon)$  from (46) in chart  $\kappa_2$  becomes

$$z_2(\epsilon) \equiv \kappa_{21}(z_1(\epsilon)) : \quad r_2 = \epsilon \nu^{-1}, \quad w_2 = w_{1c} \nu + \mathcal{O}(\epsilon), \quad \epsilon_2 = \nu,\tag{49}$$

using (39). Clearly  $z_2(\epsilon) \in \kappa_{21}(\Lambda_1) \subset U_2$ ,  $\kappa_{21}(\Lambda_1)$  being the face of the box  $U_2$  with  $\epsilon_2 = \nu$ . In this section we will for simplicity write subsets such as  $\{(\epsilon_2, w_2, \theta, \phi, v, r_2) \in U_2 | \dots\}$  by  $\{U_2 | \dots\}$ .

**Lemma 2** *The set  $M_2 = \{U_2 | r_2 = 0, \epsilon_2 = 0, w_2 = -\lambda_+\}$  is a set of critical points of (48). Linearization around  $M_2$  gives only three non-zero eigenvalues  $-\lambda_+ < 0$ ,  $\lambda_- - \lambda_+ < 0$ ,  $\lambda_+ > 0$ , and so  $M_2$  is of saddle-type. The stable manifold is  $W^s(M_2) = \{U_2 | r_2 = 0\}$  while the unstable manifold is  $W^u(M_2) = \{U_2 | \epsilon_2 = 0, w_2 = -\lambda_+\}$ . In particular, the 1D unstable manifold  $\gamma_2^u(\theta_0, \phi_0, v_0) \subset W^u(M_2)$  of the base point  $(\epsilon_2, w_2, \theta, \phi, v, r_2) = (0, 0, \theta_0, \phi_0, v_0, 0) \in M_2$  is given by*

$$\begin{aligned}\gamma_2^u(\theta_0, \phi_0, v_0) &= \left\{ U_2 | \quad w_2 = -\lambda_+(\theta_0), \quad \theta = \theta_0, \quad \phi = \phi_0 - \frac{c_+(\theta_0)}{p_+(\theta_0)} \lambda_+(\theta_0) r_2, \right. \\ &\quad \left. v = v_0 - \frac{q_+(\theta_0)}{p_+(\theta_0)} \lambda_+(\theta_0) r_2, \quad r_2 \geq 0, \quad \epsilon_2 = 0 \right\}.\end{aligned}\tag{50}$$

**PROOF** The first two statements follow from straightforward calculation. For  $\gamma_2^u(\theta_0, \phi_0, v_0)$ , we restrict to the invariant set:  $\epsilon_2 = 0, w_2 = -\lambda_+$  and solve the resulting reduced system. ■

**Remark 6** Notice that the set  $\gamma_2^u(\theta_0, \phi_0, v_0)$  is just  $\gamma^u(\theta_0, \phi_0, v_0)$  in (32) written in chart  $\kappa_2$  for  $\epsilon_2 = 0$ . □

Notice that  $z_2(0) \subset W^s(M_2)$ . The forward flow of  $z_2(0)$  is described for  $\tau \geq \tau_c$  by writing solution (47) to the layer problem  $(42)_{\epsilon=0}$  in chart  $\kappa_2$  using  $\kappa_{21}$ , to get

$$\begin{aligned}\epsilon_2(\tau) &= - \left( \frac{b(\theta_0, \phi_0)}{p_+(\theta_0)} + k_+ e^{\lambda_+ \tau} + k_- e^{\lambda_- \tau} \right)^{-1} \\ &= -k_+^{-1} e^{-\lambda_+ \tau} (1 + \mathcal{O}(e^{-\lambda_+ \tau} + e^{(\lambda_- - \lambda_+) \tau})), \quad \tau \rightarrow \infty \\ w_2(\tau) &= - (k_+ \lambda_+ e^{\lambda_+ \tau} + k_- \lambda_- e^{\lambda_- \tau}) \left( \frac{b(\theta_0, \phi_0)}{p_+(\theta_0)} + k_+ e^{\lambda_+ \tau} + k_- e^{\lambda_- \tau} \right)^{-1} \\ &= -\lambda_+ (1 + \mathcal{O}(e^{-\lambda_+ \tau} + e^{(\lambda_- - \lambda_+) \tau})), \quad \tau \rightarrow \infty.\end{aligned}\tag{51}$$

In the subsequent lemma we follow  $z_2(\epsilon) \subset \{\epsilon_2 = \nu\}$  up until  $r_2 = \nu$ , with  $\nu$  sufficiently small, by applying Fenichel's normal form theory.

**Lemma 3** *Let  $c \in (0, 1)$  and set  $\Lambda_2 = \{U_2 | r_2 = \nu\}$ . Then for  $\nu$  and  $\rho$  sufficiently small, the forward flow of  $z_2(\epsilon)$  in (49) intersects  $\Lambda_2$  in*

$$\left\{ \Lambda_2 \mid \begin{aligned} w_2 &= -\lambda_+ + \mathcal{O}(\epsilon^c), & \theta &= \theta_0 + \mathcal{O}(\epsilon \ln \epsilon^{-1}), & \phi &= \phi_0 - \frac{c_+(\theta_0)}{p_+(\theta_0)} \lambda_+(\theta_0) \nu + \mathcal{O}(\epsilon^c), \\ v &= v_0 - \frac{q_+(\theta_0)}{p_+(\theta_0)} \lambda_+(\theta_0) \nu + \mathcal{O}(\epsilon^c) \end{aligned} \right\}. \quad (52)$$

□

as  $\epsilon \rightarrow 0$ .

**PROOF** By Fenichel's normal form theory we can make the slow variables independent of the fast variables  $(\epsilon_2, w_2, r_2)$ :

**Lemma 4** *For  $\nu$  and  $\rho$  sufficiently small, then within  $U_2$  there exists a smooth transformation  $(\epsilon_2, w_2, \phi, v, r_2) \mapsto (\tilde{\phi}, \tilde{v})$  satisfying*

$$\begin{aligned} \tilde{\phi} &= \phi + \frac{c_+(\theta)}{p_+(\theta)} \lambda_+(\theta) r_2 + \mathcal{O}(r_2(w_2 + \lambda_+)), \\ \tilde{v} &= v + \frac{q_+(\theta)}{p_+(\theta)} \lambda_+(\theta) r_2 + \mathcal{O}(r_2(w_2 + \lambda_+) + \epsilon), \end{aligned} \quad (53)$$

which transforms (48) into

$$\begin{aligned} \epsilon'_2 &= \epsilon_2 w_2, \\ w'_2 &= \epsilon_2 b(\theta, \tilde{\phi}) + p_+(\theta) (1 - \delta w_2) + w_2^2 + \mathcal{O}(\epsilon), \\ \theta' &= \epsilon \tilde{\phi}, \\ \tilde{\phi}' &= 0, \\ \tilde{v}' &= 0, \\ r'_2 &= -r_2 w_2. \end{aligned} \quad (54)$$

□

**PROOF** Replace  $r_2$  by  $\nu r_2$  in (48) and consider  $\nu$  small. Then  $\epsilon_2 = r_2 = 0$ ,  $w_2 = -\lambda_+$  is a saddle-type slow manifold for  $\nu$  small. The result then follows from Fenichel's normal form theory [14]. Using  $\phi = \tilde{\phi} + \mathcal{O}(r_2)$  together with  $r_2 \epsilon_2 = \epsilon$  in the  $w_2$ -equation then gives the desired result.

To prove Lemma 3 we then integrate the normal form (54) with initial conditions  $z_2(\epsilon)$  from (49) from (a reset) time  $\tau = 0$  up to  $\tau = T$ , defined implicitly by  $r_2(T) = \nu$ . Clearly  $\theta(T) = \theta_0 + \mathcal{O}(\epsilon T)$ ,  $\tilde{\phi}(T) = \tilde{\phi}_0$ ,  $\tilde{v}(T) = \tilde{v}_0$ . Then, from (51), Gronwall's inequality and the fact that  $1 - \lambda_- \lambda_+^{-1} > 1$ , we find

$$T = \lambda_+^{-1} \ln \epsilon^{-1} (1 + o(1)) \quad (55)$$

$$\epsilon_2(T) = \epsilon \nu^{-1}$$

$$w_2(T) = -\lambda_+ (1 + \mathcal{O}(e^{-\lambda_+ T} + e^{(\lambda_- - \lambda_+) T} + \epsilon)) = -\lambda_+ + \mathcal{O}(\epsilon^{c(1 - \lambda_- \lambda_+^{-1})} + \epsilon^c) = -\lambda_+ + \mathcal{O}(\epsilon^c), \quad (56)$$



for  $c \in (0, 1)$ . Then we obtain the expressions for  $\theta = \theta(T)$ ,  $\phi = \phi(T)$  and  $v = v(T)$  in (52) from (53) in terms of the original variables. ■

#### 4.2.4 Completing the proof of Proposition 3

To complete the proof of Proposition 3 we then return to (30) using (38) and integrate initial conditions (52) within  $\{\hat{y} = -r_2 = -\nu\}$ , up to  $\Pi : v = 0$  given in (35), using regular perturbation theory and the implicit function theorem. This gives (36) which completes the proof of Proposition 3.

### 4.3 Sticking

After the slipping compression phase of the previous section, the rod then sticks on the sliding manifold  $\Pi$  given in (35), with  $(\hat{y}, w, \theta, \phi)$  given by (36). This is a corollary of the following lemma:

**Lemma 5** *Suppose  $a \neq 0$ ,  $q_+ < 0$ ,  $q_- > 0$ . Consider the (negative) function*

$$\mathcal{F}(\theta, \phi) = \begin{cases} \frac{a(\theta, \phi)}{q_+(\theta)} & \text{if } a > 0, \\ \frac{a(\theta, \phi)}{q_-(\theta)} & \text{if } a < 0. \end{cases}$$

*Then there exists a set of visible folds at:*

$$\Gamma_\epsilon \equiv \{(\hat{y}, w, \theta, \phi, v) \in \Pi \mid \hat{y} + \delta w = \epsilon \mathcal{F}(\theta, \phi)\}, \quad (57)$$

*of the Filippov system (30), dividing the switching manifold  $\Pi : v = 0$  into (stable) sticking:  $\Pi_s \equiv \{(\hat{y}, w, \theta, \phi, v) \in \Pi \mid \hat{y} + \delta w < \epsilon \mathcal{F}(\theta, \phi)\}$ , and crossing upwards (downwards) for  $a > 0$  ( $a < 0$ ):  $\Pi_c \equiv \{(\hat{y}, w, \theta, \phi, v) \in \Pi \mid \hat{y} + \delta w > \epsilon \mathcal{F}(\theta, \phi)\}$ . □*

**PROOF** Simple computations, following [11]; see also Proposition 1. ■

The forward motion of (36) within  $\Pi_s \subset \Pi$  for  $\epsilon \ll 1$  is therefore subsequently described by the Filippov vector-field (8) in Proposition 1

$$\begin{aligned} \hat{y}' &= w, \\ w' &= \epsilon b(\theta, \phi) + S_w(\theta) [-\hat{y} - \delta w], \\ \theta' &= \epsilon \phi, \\ \phi' &= S_\phi(\theta) [-\hat{y} - \delta w], \end{aligned} \quad (58)$$

here written in terms of  $\hat{y}$  and the fast time  $\tau$ , until sticking ends at the visible fold  $\Gamma_\epsilon$ . Note this always occurs for  $0 < \epsilon \ll 1$  since  $\hat{y}'' = w' > 0$ , for  $[-\hat{y} - \delta w] > 0$ .

We first focus on  $\epsilon = 0$ . From (58),  $\theta = \theta_0$ , a constant, and

$$\begin{aligned} \hat{y}' &= w, \\ w' &= S_w(\theta) [-\hat{y} - \delta w], \\ \phi' &= S_\phi(\theta) [-\hat{y} - \delta w]. \end{aligned} \quad (59)$$

We now integrate (59), using (36) for  $\epsilon = 0$  as initial conditions, given by

$$(\hat{y}(0), w(0), \phi(0)) = \left( -\frac{p_+(\theta_0)}{q_+(\theta_0)\lambda_+(\theta_0)}v_0, -\frac{p_+(\theta_0)}{q_+(\theta_0)}v_0, \phi_0 - \frac{c_+(\theta_0)}{q_+(\theta_0)}v_0 \right), \quad (60)$$

up until the section  $\Gamma_0 : \hat{y} + \delta w = 0$  shown in Fig. 3(a), where sticking ceases for  $\epsilon = 0$ , by Lemma 5 and (57) $_{\epsilon=0}$ . We then obtain a function  $e(\delta, \theta_0) > 0$  in the following proposition, which relates the horizontal velocity at the start of the slipping compression phase  $v_0$  (21) with the values of  $(\hat{y}, w, \phi)$  on  $\Gamma_0$ , at the end of the sticking phase.

**Proposition 4** *There exists a smooth function  $e(\delta, \theta_0) > 0$  and a time  $\tau_s > 0$  such that:  $(\hat{y}(\tau_s), w(\tau_s), \phi(\tau_s)) \in \Gamma_0$  with*

$$\begin{aligned} \hat{y}(\tau_s) &= -\delta e(\delta, \theta_0)v_0, \\ w(\tau_s) &= e(\delta, \theta_0)v_0, \\ \phi(\tau_s) &= \phi_0 + \left\{ -\frac{c_+(\theta_0)}{q_+(\theta_0)} + \frac{S_\phi(\theta_0)}{S_w(\theta_0)} \left( e(\delta, \theta_0) + \frac{p_+(\theta_0)}{q_+(\theta_0)} \right) \right\} v_0, \end{aligned} \quad \square$$

where  $(\hat{y}(\tau), w(\tau), \phi(\tau))$  is the solution of (59) with initial conditions (60). The function  $e(\delta, \theta_0)$  is monotonic in  $\delta$ :  $\partial_\delta e(\delta, \theta_0) < 0$ , and satisfies (24) and (25) for  $\delta \gg 1$  and  $\delta \ll 1$ , respectively.

**PROOF** The existence of  $\tau_s$  is obvious. Linearity in  $v_0$  follows from (60) and the linearity of (59). Since  $\dot{\hat{y}} = w$ , we have  $e > 0$ . The  $\phi$ -equation follows since  $\phi' = \frac{S_\phi(\theta)}{S_w(\theta)}w'$ . The monotonicity of  $e$  as function  $\delta$  is the consequence of simple arguments in the  $(w, \hat{y})$ -plane using (59) and the fact that  $w(0)$  in (60) is independent of  $\delta$  while  $\hat{y}(0) = \hat{y}_0(\delta)$  decreases (since  $\lambda_+$  is an increasing function of  $\delta$ ). To obtain the asymptotics we first solve (59) with  $\delta \neq \frac{2}{\sqrt{S_w(\theta_0)}}$ . Simple calculations show that

$$e(\delta, \theta_0) = \frac{\xi_+}{\xi_-} (\lambda_+ - \xi_-) \frac{p_+}{q_+ \lambda_+} e^{\xi_+ \tau_s}, \quad (61)$$

suppressing the dependency on  $\theta_0$  on the right hand side, where  $\xi_\pm = -\frac{\delta S_w}{2} \pm \frac{1}{2} \sqrt{\delta^2 S_w^2 - 4S_w}$ , and  $\tau_s$  is the least positive solution of  $e^{(\xi_+ - \xi_-)\tau_s} = \frac{\xi_-^2 (\lambda_+ - \xi_+)}{\xi_+^2 (\lambda_+ - \xi_-)}$ . For  $\delta \gg 1$  the eigenvalues  $\xi_\pm$  are real and negative. Hence  $\tau_s = \frac{1}{\xi_+ - \xi_-} \ln \left( \frac{\xi_-^2 (\lambda_+ - \xi_+)}{\xi_+^2 (\lambda_+ - \xi_-)} \right)$ . Now using  $\xi_+ = -S_w \delta (1 + \mathcal{O}(\delta^{-2}))$ ,  $\xi_- = \frac{S_w}{\xi_+} = -\delta^{-1} (1 + \mathcal{O}(\delta^{-1}))$ , and  $\lambda_+ = -p_+ \delta (1 + \mathcal{O}(\delta^{-2}))$ , we obtain  $\xi_+ \tau_s = \mathcal{O}(\delta^{-2} \ln \delta^{-1})$ , and hence

$$e(\delta, \theta_0) = -\frac{S_w - p_+}{q_+ S_w} \delta^{-2} (1 + \mathcal{O}(\delta^{-2} \ln \delta^{-1})), \quad (62)$$

as  $\delta \rightarrow \infty$ . For  $\delta \ll 1$ ,  $\xi_\pm$  are complex conjugated with negative real part. This gives  $\tau_s = \frac{2i}{\xi_+ - \xi_-} (\phi - \pi n)$ ,  $\phi = \arg((\lambda_+ - \xi_+) \xi_-^2) > 0$ ,  $n = \lfloor \phi/\pi \rfloor$ . Using the asymptotics of  $\xi_\pm$

and  $\lambda_+$  we obtain  $\tau_s = \frac{\pi - \arctan\left(\sqrt{-\frac{S_w}{p_+}}\right)}{\sqrt{S_w}} - \frac{1}{2}\delta(1 + \mathcal{O}(\delta))$ , and then

$$e(\delta, \theta_0) = -\frac{\sqrt{p_+(p_+ - S_w)}}{q_+} \left( 1 - \frac{\sqrt{S_w}}{2} \left( \pi - \arctan\left(\sqrt{-\frac{S_w}{p_+}}\right) \right) \delta + \mathcal{O}(\delta^2) \right), \quad (63)$$

as  $\delta \rightarrow 0^+$ . Simple algebraic manipulations of (62) and (63) using (9) give the expressions in (24) and (25).  $\blacksquare$

**Remark 7** The critical value  $\delta = \delta_{crit}(\theta_0) \equiv \frac{2}{\sqrt{S_w(\theta_0)}}$  gives a double root of the characteristic equation. Note that  $\delta_{crit}(\frac{\pi}{2}) = 2$  for the classical Painlevé problem, as expected (see section 2.2).  $\square$

For  $0 < \epsilon \ll 1$  sticking ends along the visible fold at  $\Gamma_\epsilon$ . We therefore perturb from  $\epsilon = 0$  as follows:

**Proposition 5** *The forward flow of (36) under the Filippov vector-field (58) intersects the set of visible folds  $\Gamma_\epsilon$   $o(1)$ -close to the intersection of  $(36)_{\epsilon=0}$  with  $\Gamma_0$  described in Proposition 4.*  $\square$

**PROOF** Since the  $\epsilon = 0$  system is transverse to  $\Gamma_0$  we can apply regular perturbation theory and the implicit function theorem to perturb  $\tau_s$  continuously to  $\tau_s + o(1)$ . The result then follows.  $\blacksquare$

#### 4.4 Lift-off

Beyond  $\Gamma_\epsilon$  we have  $\hat{F}_N \equiv 0$  and lift-off occurs. For  $\epsilon = 0$  we have  $\hat{y}' = w$  and  $w' = \theta' = \phi' = v' = 0$ . By Proposition 5 and regular perturbation theory, we obtain the desired result in Theorem 1. In terms of the original (slow) time  $t$ , it follows that the time of IWC is of order  $\mathcal{O}(\epsilon \ln \epsilon^{-1})$  (recall (55)). As  $\epsilon \rightarrow 0$ , IWC occurs instantaneously, as desired.

### 5 Proof of Theorem 2: IWC in the indeterminate case

Here, by assumption (27), we have  $b > 0$ . Now  $C_1 \subset \{\hat{y}_1 < 0\}$ , where  $C_1$  is given by (43); see also Fig. 4(b). The stable manifold of  $C_1 \cap \{\theta = \theta_0, \phi = \phi_0, v = v_0\}$  is:

$$\gamma_1^s(\theta_0, \phi_0, v_0) = \left\{ (\hat{y}_1, w_1, \theta_0, \phi_0, v_0) \mid \hat{y}_1 = \frac{b(\theta_0, \phi_0)}{p_+(\theta_0)} + s, \quad w_1 = \lambda_-(\theta_0)s, \quad s \leq -\frac{b(\theta_0, \phi_0)}{p_+(\theta_0)}, \right\} \quad (64)$$

with  $\lambda_-$  defined in (33).  $\gamma_1^s$  intersects the  $w_1$ -axis in

$$\gamma_1^s \cap \{\hat{y}_1 = 0\} : \quad w_1 = w_{1*} \equiv -\lambda_-(\theta_0) \frac{b(\theta_0, \phi_0)}{p_+(\theta_0)} < 0, \quad (65)$$

and divides the negative  $w_1$ -axis into (i) initial conditions that lift off directly ( $w_{10} > w_{1*}$ , blue in Fig. 4(b)) and (ii) initial conditions that undergo IWC before returning to  $\hat{y} = 0$  ( $w_{10} < w_{1*}$ , green in Fig. 4(b)). (A canard phenomenon occurs around  $w_{10} = w_{1*}$  for  $0 < \epsilon \ll 1$  where the solution follows a saddle-type slow manifold for an extended period of time.) For  $w_{10} < w_{1*}$  the remainder of the proof of Theorem 2 on IWC in the indeterminate case then follows the proof of Theorem 1 above.

## 6 Discussion

The quantity  $e(\delta, \theta_0)$  relates the initial horizontal velocity  $v_0$  of the rod to the resulting vertical velocity at the end of IWC. It is like a “horizontal coefficient of restitution”. The leading order expression of  $e(\delta, \theta_0)$  in (24) for  $\delta \gg 1$  is independent of  $\mu$ , in general. Using the expressions for  $q_{\pm}$  and  $p_{\pm}$  in (6), together with (62), we find for large  $\delta$  that

$$e(\delta, \theta_0) = \frac{\alpha}{2(1+\alpha)} \sin(2\theta_0) \delta^{-2} (1 + \mathcal{O}(\delta^{-2} \ln \delta^{-1})), \quad \theta_0 \in (\theta_1, \theta_2). \quad (66)$$

The limit  $\delta \rightarrow \infty$  is not uniform in  $\theta \in (\theta_1, \theta_2)$ .

The expression for  $\delta \ll 1$  is more complicated and *does* depend upon  $\mu$ , in general. Using (6) and (63), for  $\delta = 0$ , we have:

$$e(0, \theta_0) = \sqrt{\frac{(1 + \alpha \cos^2 \theta_0 - \mu \alpha \sin \theta_0 \cos \theta_0)}{(\alpha \sin \theta_0 \cos \theta_0 - \mu(1 + \alpha \sin^2 \theta_0))} \frac{\alpha \sin \theta \cos \theta_0}{(1 + \alpha \sin^2 \theta_0)}} \quad (67)$$

We plot  $e(0, \theta_0)$  in Fig. 5(a) for  $\alpha = 3$  and  $\mu = 1.4$ . Fig. 5(b) shows the graph of  $e(\delta, 1)$  and  $e(\delta, 1.2)$  along with the approximations (dashed lines) in (24) and (25).

In the inconsistent case, described by Theorem 1, the initial conditions (21) are very similar to those assumed by [37]. As in their case, these conditions would be impossible to reach in an experiment without using some form of controller<sup>5</sup>. Nevertheless, it should be possible to set up the initial conditions in (21) to approach the rigid surface from above, as it appears to have been done in [38] for the two-link manipulator system.

The indeterminate case described by Theorem 2 is characterised by an extreme exponential splitting in phase space, due to the stable manifold of  $C_1$  in the  $\kappa_1$ -system (43). For example, the blue orbit in Fig. 4(b) lifts off directly with  $w = \mathcal{O}(\epsilon)$ . But on the other side of the stable manifold, the green orbit undergoes IWC and then lifts off with  $w = \mathcal{O}(1)$ . The initial conditions in Theorem 2 correspond to orbits that are almost grazing ( $\dot{y} = w = \mathcal{O}(\epsilon)$ ,  $\ddot{y} = \dot{w} = b > 0$ ) the compliant surface at  $y = 0$ . In Fig. 6 we illustrate this further by computing the full Filippov system (5) <sub>$\epsilon=10^{-3}$</sub>  for two rods (green and blue) initially distant by an amount of  $10^{-3}$  above the compliant surface ( $y \approx 0.1$ , see also  $t = 0$  in Fig. 6(a)). Fig. 6(a) shows the configuration of the rods at different times  $t = 0$ ,  $t = 0.25$ ,

---

<sup>5</sup>To see this, fix any  $\hat{y}_0 < 0$ . Then by applying the approach in section 4.2 backwards in time, it follows that the backward flow of (21) for  $b < 0$  (dashed lines in Fig. 4(a), illustrating the  $\kappa_1$ -dynamics) intersects the section  $\{\hat{y} = \hat{y}_0\}$  at a distance which is  $o(1)$ -close to  $\gamma^s \cap \{\hat{y} = \hat{y}_0\}$  as  $\epsilon \rightarrow 0$ . Here  $\gamma^s$  is the stable manifold of  $C$  for  $\epsilon = 0$ . But cf. (30) <sub>$\epsilon=0$</sub> , the horizontal velocity  $v$  (and hence the energy) increases unboundedly along  $\gamma^s$  in backwards time. This increase occurs on the fast time scale  $\tau$ .

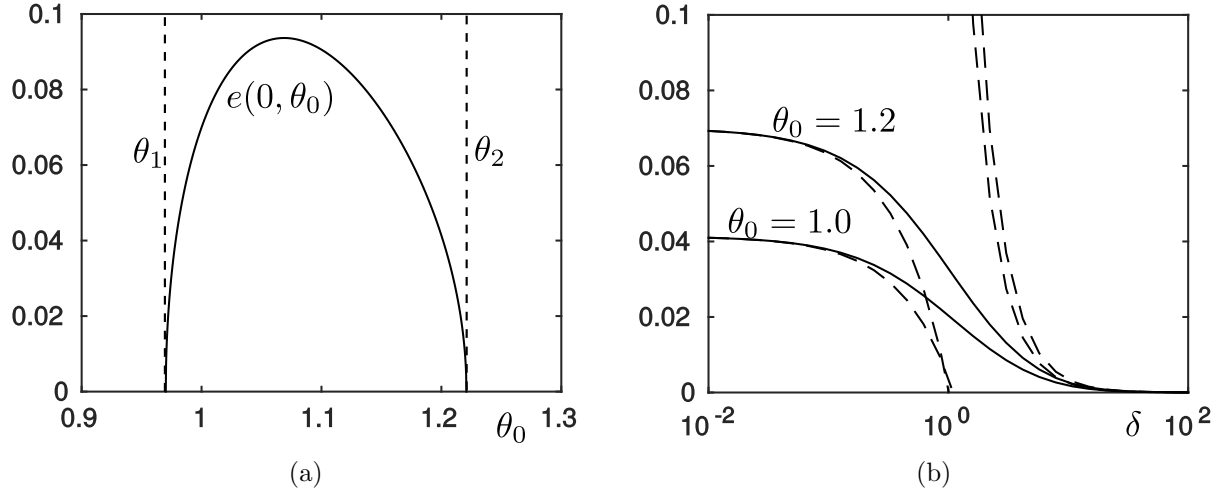


Figure 5: (a) Graph of  $e(0, \theta_0)$  from (67), where  $\theta_{1,2}$  are given by (14). (b) Graph of  $e(\delta, \theta_0)$  for  $\theta_0 = 1$  and  $\theta_0 = 1.2$ , where the dashed lines correspond to the approximations obtained from (24) and (25). For both figures,  $\alpha = 3$  and  $\mu = 1.4$ .

$t = 0.5$  and  $t = 1$ . Up until  $t = 0.5$ , the two rods are indistinguishable. At  $t = 0.5$ , grazing ( $\dot{y} = w \approx 10^{-3}$ ) with the compliant surface  $y = 0$  occurs where  $\theta \approx 0.9463$ ,  $\phi \approx 1.6654$ ,  $v \approx 1.00$  (so  $b \approx 1.2500$  and  $p_+ \approx -2.243$ ). The green rod then undergoes IWC, occurring on the fast time scale  $\tau$ , and therefore subsequently lifts off from  $y = 0$  with  $w = \mathcal{O}(1)$ . In comparison the blue rod lifts off with  $w \approx 10^{-3}$ . At  $t = 1$  the two rods are clearly separated. Fig. 6(b) shows the projection of the numerical solution in Fig. 6(a) onto the  $(w, \hat{y})$ -plane (compare Fig. 3(b)). The blue orbit lifts off directly. The green orbit, being on the other side of the stable manifold of  $C_1$ , follows the unstable manifold (red) until sticking occurs. Then when  $\hat{F}_N = 0$  at  $\hat{y} + \delta \hat{w} = 0$  (dashed line), lift off occurs almost vertically in the  $(w, \hat{y})$ -plane. Fig. 6(c) and Fig. 6(d) show the vertical velocity  $w$  and horizontal velocity  $v$ , respectively, for both orbits over the same time interval as Fig. 6(b); note the sharp transition for the green orbit around  $t = 0.5$ , as it undergoes IWC. In Fig. 6(c), we include two dashed lines  $w = ev_0$  and  $w = -\frac{p_+}{q_+}v_0$ , corresponding to our analytical results (23) and (36), which also hold for the indeterminate case (from Theorem 2), in excellent agreement with the numerical results.

## 7 Conclusions

We have considered the problem of a rigid body, subject to a unilateral constraint, in the presence of Coulomb friction. Our approach was to regularize the problem by assuming a compliance with stiffness and damping at the point of contact. This leads to a slow-fast system, where the small parameter  $\epsilon$  is the inverse of the square root of the stiffness.

Like other authors, we found that the fast time scale dynamics is unstable. Dupont and Yamajako [7] established conditions in which these dynamics can be stabilized. In contrast,

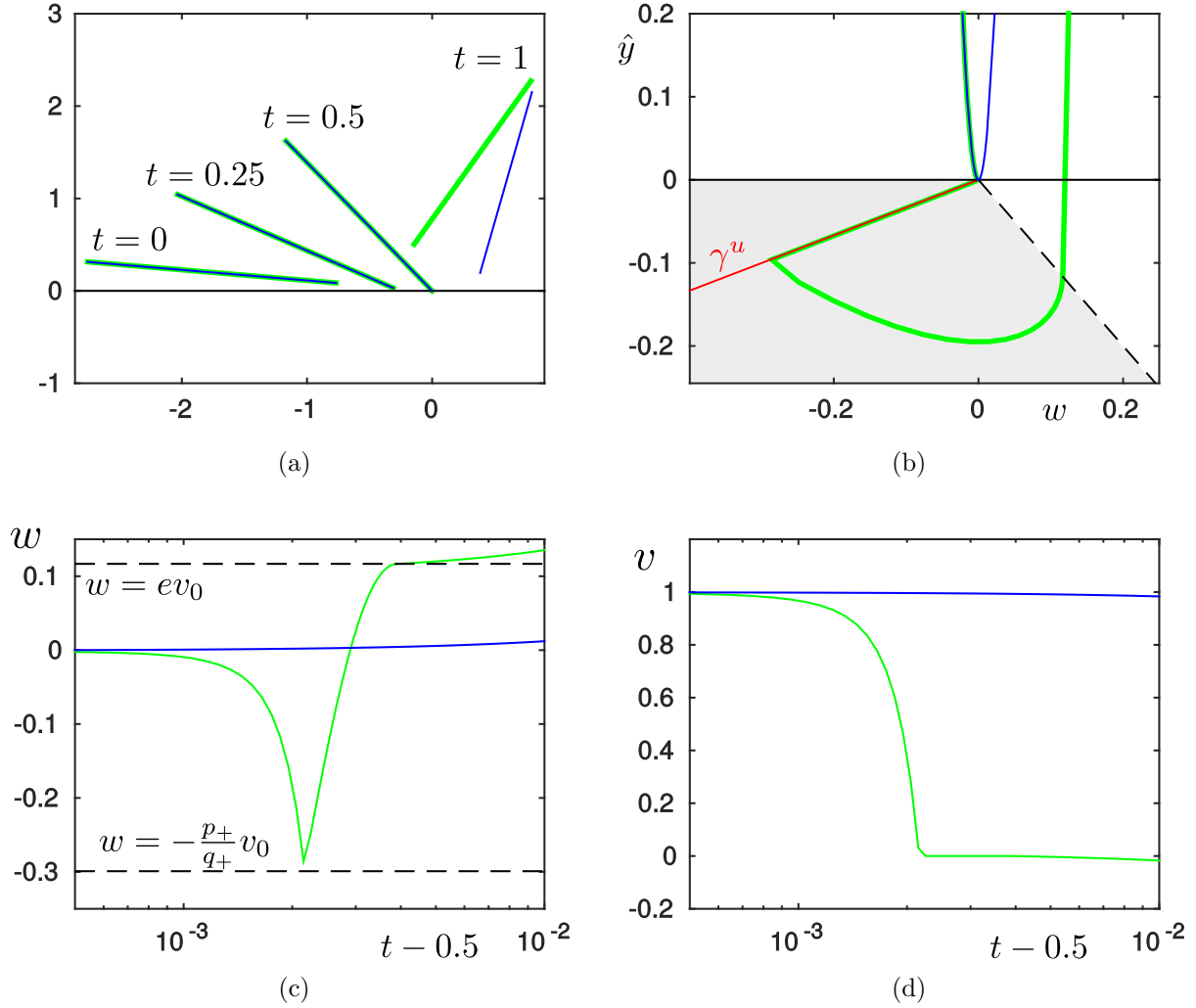


Figure 6: (a) Dynamics of the Painlevé rod described by the Filippov system (5) for  $\mu = \alpha = 3$ ,  $\delta = 1$  and  $\epsilon = 10^{-3}$  in the indeterminate case. The green and blue rods are separated at  $t = 0$  by a distance of  $10^{-3}$ . At around  $t = 0.5$ , impact with the compliant surface occurs. The green rod experiences IWC whereas the blue rod lifts off directly. (b) Projection onto the  $(w, \hat{y})$ -plane. (c) and (d)  $w$  and  $v$  as functions of time near  $t = 0.5$ .

McClamroch [24] established under what conditions the unstable fast time scale dynamics could be controlled by the slow time scale dynamics. Other authors have used the initial scaling (28), together with the scaling  $\kappa_1$  to numerically compute stability boundaries [7, 24] or phase plane diagrams [5].

The main achievement of this paper is to rigorously derive these, and other, results that have eluded others in simpler settings. For example, the work of Zhao *et al.* [37] assumes no damping in the compliance and uses formal methods to provide estimates of the times spent in the three phases of IWC. They suggest that their analysis can “... roughly explain why the Painlevé paradox can result in [IWC].”. In contrast, we assumed that the compliance has

both stiffness and damping, analysed the problem rigorously, derived exact and asymptotic expressions for many important quantities in the problem and showed *exactly* how and why the Painlevé paradox can result in IWC. There are no existing results comparable to (23), (24) and (25) for any value of  $\delta$ .

Our results are presented for arbitrary values of the compliance damping and we are able to give explicit asymptotic expressions in the limiting cases of small and large damping, all for a large class of rigid bodies, including the case of the classical Painlevé example in Fig. 1.

Given a general class of rigid body and a general class of normal reaction, we have been able to derive an explicit connection between the initial horizontal velocity of the body and its lift-off vertical velocity, for arbitrary values of the compliance damping, as a function of the initial orientation of the body.

## References

- [1] Le Suan An. The Painlevé paradoxes and the law of motion of mechanical systems with Coulomb friction. *Prikl. Math. Mekh.*, 54:430–438, 1990.
- [2] A. Blumenthals, B. Brogliato, and F. Bertails-Descoubes. The contact problem in Lagrangian systems subject to bilateral and unilateral constraints, with or without sliding Coulomb’s friction: a tutorial. *Multibody Syst. Dyn.*, 38:43–76, 2016.
- [3] R.M. Brach. Impacts coefficients and tangential impacts. *ASME J. Applied Mechanics*, 64:1014–1016, 1997.
- [4] B. Brogliato. *Nonsmooth mechanics*. Springer, London, 2nd edition, 1999.
- [5] A.R. Champneys and P. Várkonyi. The Painlevé paradox in contact mechanics. *IMA J. Applied Math.*, 81:538–588, 2016.
- [6] G. Darboux. Étude géométrique sur les percussions et le choc des corps. *Bulletin des Sciences Mathématiques et Astronomique, 2e serie*, 4:126–160, 1880.
- [7] P. E. Dupont and S. P. Yamajako. Stability of frictional contact in constrained rigid-body dynamics. *IEEE Trans. Robotics Automation*, 13:230–236, 1997.
- [8] N. Fenichel. Persistence and smoothness of invariant manifolds for flows. *Indiana University Mathematics Journal*, 21:193–226, 1971.
- [9] N. Fenichel. Asymptotic stability with rate conditions. *Indiana University Mathematics Journal*, 23:1109–1137, 1974.
- [10] N. Fenichel. Geometric singular perturbation theory for ordinary differential equations. *J. Diff. Eq.*, 31:53–98, 1979.
- [11] A.F. Filippov. *Differential Equations with Discontinuous Righthand Sides*. Mathematics and its Applications. Kluwer Academic Publishers, 1988.

- [12] F. Génot and B. Brogliato. New results on Painlevé paradoxes. *European Journal of Mechanics A/Solids*, 18:653–677, 1999.
- [13] A.P. Ivanov. On the correctness of the basic problem of dynamics in systems with friction. *Prikl. Math. Mekh.*, 50:547–550, 1986.
- [14] C.K.R.T. Jones. *Geometric Singular Perturbation Theory, Lecture Notes in Mathematics, Dynamical Systems (Montecatini Terme)*. Springer, Berlin, 1995.
- [15] J. B. Keller. Impact with friction. *ASME J. Applied Mechanics*, 53:1–4, 1986.
- [16] K. Uldall Kristiansen and S. J. Hogan. On the use of blowup to study regularizations of singularities of piecewise smooth dynamical systems in  $\mathbb{R}^3$ . *SIAM Journal on Applied Dynamical Systems*, 14(1):382–422, 2015.
- [17] K. Uldall Kristiansen and S. J. Hogan. Regularizations of two-fold bifurcations in planar piecewise smooth systems using blowup. *SIAM Journal on Applied Dynamical Systems*, 14(4):1731–1786, 2015.
- [18] K. Uldall Kristiansen and S. J. Hogan. Le canard de Painlevé. *In preparation*, 2017.
- [19] M. Krupa and P. Szmolyan. Extending geometric singular perturbation theory to non-hyperbolic points - fold and canard points in two dimensions. *SIAM Journal on Mathematical Analysis*, 33(2):286–314, 2001.
- [20] C. Kuehn. *Multiple Time Scale Dynamics*. Springer-Verlag, Berlin, 2015.
- [21] L. Lecornu. Sur la loi de Coulomb. *Comptes Rendu des Séances de l’Academie des Sciences*, 140:847–848, 1905.
- [22] R. Leine, B. Brogliato, and H. Nijmeijer. Periodic motion and bifurcations induced by the Painlevé paradox. *European Journal of Mechanics A/Solids*, 21:869–896, 2002.
- [23] C. Liu, Z. Zhao, and B. Chen. The bouncing motion appearing in a robotic system with unilateral constraint. *Nonlinear Dynamics*, 49:217–232, 2007.
- [24] N. H. McClamroch. A singular perturbation approach to modeling and control of manipulators constrained by a stiff environment. In *Proc. 28th Conf. Decision Contr.*, pages 2407–2411, December 1989.
- [25] Yu. I. Neimark and N. A. Fufayev. The Painlevé paradoxes and the dynamics of a brake shoe. *J. Applied Math. Mech.*, 59:343–352, 1995.
- [26] Yu. I. Neimark and V. N. Smirnova. Contrast structures, limit dynamics and the Painlevé paradox. *Differential Equations*, 37:1580–1588, 2001.
- [27] Y. Or. Painlevé’s paradox and dynamic jamming in simple models of passive dynamic walking. *Regular and Chaotic Dynamics*, 19:64–80, 2014.



- [28] Y. Or and E. Rimon. Investigation of Painlevé’s paradox and dynamic jamming during mechanism sliding motion. *Nonlinear Dynamics*, 67:1647–1668, 2012.
- [29] P. Painlevé. Sur les loi du frottement de glissement. *Comptes Rendu des Séances de l’Academie des Sciences*, 121:112–115, 1895.
- [30] P. Painlevé. Sur les loi du frottement de glissement. *Comptes Rendu des Séances de l’Academie des Sciences*, 141:401–405, 1905.
- [31] P. Painlevé. Sur les loi du frottement de glissement. *Comptes Rendu des Séances de l’Academie des Sciences*, 141:546–552, 1905.
- [32] Y. Shen and W. J. Stronge. Painlevé’s paradox during oblique impact with friction. *European Journal of Mechanics A/Solids*, 30:457–467, 2011.
- [33] P. Song, P. Kraus, V. Kumar, and P. E. Dupont. Analysis of rigid-body dynamic models for simulation of systems with frictional contacts. *ASME J. Applied Mechanics*, 68:118–128, 2001.
- [34] D. E. Stewart. Rigid-body dynamics with friction and impact. *SIAM Review*, 42:3–39, 2000.
- [35] W. J. Stronge. Energetically consistent calculations for oblique impact in unbalanced systems with friction. *ASME J. Applied Mechanics*, 82:081003, 2015.
- [36] E. V. Wilms and H. Cohen. Planar motion of a rigid body with a friction rotor. *ASME J. Applied Mechanics*, 48:205–206, 1981.
- [37] Z. Zhao, C. Liu, B. Chen, and B. Brogliato. Asymptotic analysis and Painlevé’s paradox. *Multibody Syst. Dyn.*, 35:299–319, 2015.
- [38] Z. Zhao, C. Liu, W. Ma, and B. Chen. Experimental investigation of the Painlevé paradox in a robotic system. *ASME J. Applied Mechanics*, 75:041006, 2008.